

Partition of Unity Neural Networks for Interpretable Classification with Explicit Class Regions

Akram Aldroubi
 Department of Mathematics
 Vanderbilt University
 akram.aldrouri@vanderbilt.edu

Abstract

Despite their empirical success, neural network classifiers remain difficult to interpret. In softmax-based models, class regions are defined implicitly as solutions to systems of inequalities among logits, making them difficult to extract and visualize. We introduce Partition of Unity Neural Networks (PUNN), an architecture in which class probabilities arise directly from a learned partition of unity, without requiring a softmax layer.

PUNN constructs k nonnegative functions h_1, \dots, h_k satisfying $\sum_i h_i(x) = 1$, where each $h_i(x)$ directly represents $P(\text{class } i \mid x)$. Unlike softmax, where class regions are defined implicitly through coupled inequalities among logits, each PUNN partition function h_i directly defines the probability of class i as a standalone function of x .

We prove that PUNN is dense in the space of continuous probability maps on compact domains. The gate functions g_i that define the partition can use various activation functions (sigmoid, Gaussian, bump) and parameterizations ranging from flexible MLPs to parameter-efficient shape-informed designs (spherical shells, ellipsoids, spherical harmonics).

Experiments on synthetic data, UCI benchmarks, and MNIST show that PUNN with MLP-based gates achieves accuracy within 0.3–0.6% of standard multilayer perceptrons. When geometric priors match the data structure, shape-informed gates achieve comparable accuracy with up to $300\times$ fewer parameters. These results demonstrate that interpretable-by-design architectures can be competitive with black-box models while providing transparent class probability assignments.

Keywords: Neural networks, interpretable machine learning, probabilistic classification, partition of unity, approximation theory.

1 Introduction

Modern neural networks achieve remarkable performance on classification tasks, yet their decision-making processes remain largely opaque [LeCun et al., 2015, Goodfellow et al., 2016]. This lack of interpretability poses significant challenges in high-stakes domains such as medical diagnosis, legal decisions, and autonomous systems, where understanding *why* a model made a particular prediction is as important as the prediction itself [Lipton, 2018, Doshi-Velez and Kim, 2017].

The standard approach to neural network classification uses the softmax function to convert a vector of logits into a probability distribution [Bishop, 2006, Goodfellow et al., 2016, Hastie et al., 2009]. Specifically, given logits $z = f(x)$, the predicted class probabilities are defined by

$$P(\text{class } i \mid x) = \frac{\exp(z_i)}{\sum_{j=1}^k \exp(z_j)}. \quad (1)$$

While mathematically convenient, softmax defines class probabilities through a global competition: all logits interact through the normalization denominator. This global coupling complicates interpretability and calibration, motivating a large literature on post-hoc correction and explanation methods. [Guo et al., 2017, Plessis and Sugiyama, 2015].

Beyond softmax-based classifiers, related ideas have appeared in mixture-of-experts models, gating networks, and hierarchical classifiers, where multiple components are combined through learned selection mechanisms [Jacobs et al., 1991, Jordan and Jacobs, 1994, Shazeer et al., 2017, Kotschieder et al., 2015]. These approaches typically rely on normalization or aggregation steps to form probabilities, and the resulting class assignments are often implicit rather than explicitly decomposed into interpretable acceptance and rejection regions. In contrast, PUNN enforces probabilistic validity locally through its recursive construction, yielding explicit class regions rather than latent routing weights.

In this paper, we propose *Partition of Unity Neural Networks* (PUNN), an architecture where class probabilities arise directly from a partition of unity construction. The key insight is that if we construct functions h_1, \dots, h_k satisfying

$$\sum_{i=1}^k h_i(x) = 1 \quad \text{and} \quad h_i(x) \geq 0 \quad \text{for all } x, \quad (2)$$

then each $h_i(x)$ can be directly interpreted as $P(\text{class } i \mid x)$ without any additional transformation. PUNN achieves this through a recursive product of gate functions: each gate $g_i(x) \in [0, 1]$ determines whether an input “belongs” to class i or should be passed to subsequent classes. Unlike softmax-based classifiers or mixture-based normalization schemes, the probabilistic structure in PUNN is enforced directly at the architectural level rather than through a global normalization step.

In high-dimensional settings, direct visualization of class probability functions is infeasible for any classifier. The interpretability of PUNN therefore does not rely on visualization, but on the explicit decomposition of probabilities into acceptance and rejection functions that remain meaningful regardless of input dimension.

This construction provides *built-in interpretability*: the hierarchical structure explicitly shows which classes were rejected and why, making the decision process transparent by design rather than requiring additional explanation machinery. This stands in contrast to post-hoc explanation methods such as feature attribution or surrogate models, which seek to rationalize predictions after training rather than enforcing interpretability at the architectural level [Ribeiro et al., 2016, Lundberg and Lee, 2017, Molnar, 2020].

We demonstrate that PUNN achieves accuracy within 0.3–0.6% of standard MLPs across UCI benchmarks [Asuncion and Newman, 2007] (Iris, Wine, Breast Cancer, Digits) and reaches 97.85% on MNIST compared to 98.19% for MLPs. Crucially, this competitive performance comes with interpretable decision structure at no additional cost. We further show that shape-informed gate functions (e.g., Gaussian ellipsoids) can achieve comparable accuracy with an order of magnitude fewer parameters—28 parameters on Iris compared to over 1,300 for MLPs.

Our main contributions are:

1. **PUNN Architecture:** We introduce a neural network architecture that constructs partition functions through a recursive product of gate functions, guaranteeing valid probability distributions by construction without softmax.
2. **Approximation of Probability Maps:** We prove that PUNN is dense in the space of continuous probability maps on compact domains.

3. **Flexible Gate Parameterization:** We demonstrate that gate functions can range from simple shape-informed functions (yielding highly parameter-efficient models) to MLP-based gates (yielding maximal flexibility), providing a spectrum of interpretability-capacity trade-offs.
4. **Empirical Validation:** We show that PUNN matches MLP accuracy within 0.3% on average across six UCI datasets and MNIST, demonstrating that interpretable-by-design architectures can be competitive with black-box models.

The remainder of this paper is organized as follows. Section 2 reviews related work on partition of unity methods and interpretable machine learning. Section 4 provides theoretical analysis, including a density result for continuous probability maps. Section 5 presents experimental results on synthetic, UCI, and image classification benchmarks. Section 7 discusses limitations and future directions. Section 8 concludes.

2 Related Work

2.1 Partition of Unity Methods

Partition of unity methods have a long history in numerical analysis and approximation theory. The partition of unity finite element method [Babuška and Melenk, 1997] uses overlapping patches with partition of unity functions to construct flexible approximation spaces. Meshfree methods such as the element-free Galerkin method [Belytschko et al., 1994] rely on partition of unity constructions for function approximation without mesh constraints. Radial basis function (RBF) networks [Powell, 1987] use localized basis functions that can form partitions of unity, providing both interpolation guarantees and intuitive geometric interpretation.

PUNN draws directly from this tradition: our partition functions $h_i(x)$ satisfy the classical partition of unity property $\sum_i h_i(x) = 1$ by construction, enabling the same theoretical guarantees while operating within a neural network framework.

Related ideas have recently appeared in neural architectures that incorporate partition of unity constructions for function approximation and operator learning. For example, POUNets use partition of unity principles to localize approximation and improve convergence properties in regression settings. These approaches focus on approximating real-valued functions or operators and do not address probabilistic classification or the construction of class probabilities [Lee et al., 2021].

In contrast, PUNN uses a partition of unity to define class probabilities directly, replacing softmax normalization with an architectural guarantee of probabilistic validity. This distinction is central: in PUNN, each partition function represents a probability by construction rather than serving as a local basis for regression.

2.2 Interpretable Machine Learning

Recent work on interpretable machine learning includes Neural Additive Models (NAM) [Agarwal et al., 2021], which restrict neural networks to additive structures for interpretability. Explainable Boosting Machines [Lou et al., 2012] combine boosting with generalized additive models. Attention mechanisms [Vaswani et al., 2017] provide some interpretability through attention weights, though their faithfulness has been questioned [Jain and Wallace, 2019].

PUNN takes a different approach to interpretability. Rather than restricting model capacity or relying on post-hoc explanation methods, PUNN constructs class probabilities through a hierarchical rejection structure that is interpretable by design. Each gate function g_i determines whether an

input is assigned to class i or passed to subsequent classes, yielding an explicit accept/reject decision process that requires no additional interpretation machinery.

2.3 Approximation of Probability Maps

Universal approximation theorems establish that standard neural networks can approximate any continuous real-valued function on a compact domain to arbitrary precision. Classical results include Cybenko [1989] for sigmoidal networks and Hornik et al. [1989] for general activation functions.

Our work builds on this foundation by studying approximation within a *structured function class* relevant to classification. Rather than approximating arbitrary real-valued functions, we consider continuous *probability maps*, i.e., continuous functions taking values in the probability simplex. We show that the PUNN architecture is dense in this space, demonstrating that the partition of unity construction does not sacrifice expressive power for probabilistic classification despite imposing explicit structure and interpretability.

3 Partition of Unity Neural Networks

3.1 Architecture Definition

Let $x \in \mathbb{R}^d$ be an input. A Partition of Unity Neural Network with k partitions consists of:

1. **Gate functions:** $g_1, \dots, g_{k-1} : \mathbb{R}^d \rightarrow [0, 1]$, each parameterized as

$$g_i(x) = g(\theta_i(x)), \quad (3)$$

where $g : \mathbb{R} \rightarrow [0, 1]$ is a smooth activation function and $\theta_i : \mathbb{R}^d \rightarrow \mathbb{R}$ is a parameterized function (e.g., a neural network or a geometric primitive).

Common choices for g include:

- **Sigmoid:** $g(t) = \sigma(t) = 1/(1 + e^{-t})$
- **Gaussian:** $g(t) = \exp(-t^2)$
- **Bump:** $g(t) = \begin{cases} \exp\left(-\frac{1}{1-t^2}\right) & |t| < 1 \\ 0 & |t| \geq 1 \end{cases}$ — C^∞ with compact support

The parameterization θ_i can range from simple geometric forms to flexible neural networks:

- **MLP-based:** $\theta_i(x) = \text{MLP}_i(x)$ — maximum flexibility
- **Radial:** $\theta_i(x) = s_i(r_i - \|x - c_i\|)$ — spherical regions centered at c_i with radius r_i and scaling s_i
- **Ellipsoidal:** $\theta_i(x) = s_i(1 - (x - c_i)^\top A_i(x - c_i))$ — axis-aligned or rotated ellipsoids

2. **Partition functions:** $h_1, \dots, h_k : \mathbb{R}^d \rightarrow [0, 1]$ defined recursively as

$$h_1(x) = g_1(x), \quad (4)$$

$$h_i(x) = \left(\prod_{j=1}^{i-1} (1 - g_j(x)) \right) g_i(x), \quad i = 2, \dots, k-1, \quad (5)$$

$$h_k(x) = \prod_{j=1}^{k-1} (1 - g_j(x)). \quad (6)$$

Proposition 1 (Partition of Unity Property). *Let $k \geq 2$. For every $x \in \mathbb{R}^d$, the partition functions satisfy*

$$\sum_{i=1}^k h_i(x) = 1 \quad \text{and} \quad h_i(x) \geq 0 \quad \text{for all } i.$$

Proof. Define, for $m \geq 1$,

$$S_m(x) := \sum_{j=1}^m \left(\prod_{i=1}^{j-1} (1 - g_i(x)) \right) g_j(x),$$

with the standard convention that an empty product equals 1.

Note that, for $2 \leq l \leq k$

$$\sum_{i=1}^l h_i(x) = S_{l-1}(x) + h_l(x). \quad (7)$$

We claim that for all $m \geq 1$,

$$S_m(x) = 1 - \prod_{j=1}^m (1 - g_j(x)).$$

For $m = 1$, this is immediate since

$$S_1(x) = g_1(x) = 1 - (1 - g_1(x)).$$

Assume the identity holds for some $m \geq 1$. Then

$$\begin{aligned} S_{m+1}(x) &= S_m(x) + \prod_{j=1}^m (1 - g_j(x)) g_{m+1}(x) \\ &= 1 - \prod_{j=1}^m (1 - g_j(x)) + \prod_{j=1}^m (1 - g_j(x)) g_{m+1}(x) \\ &= 1 - \prod_{j=1}^m (1 - g_j(x)) (1 - g_{m+1}(x)) \\ &= 1 - \prod_{j=1}^{m+1} (1 - g_j(x)). \end{aligned}$$

This completes the induction.

Taking $m = k - 1$ and $l = k$ in (7), and using the definition of h_k , we obtain

$$\sum_{i=1}^k h_i(x) = 1.$$

Finally, since each $g_i(x) \in [0, 1]$, all factors defining $h_i(x)$ are nonnegative, and hence $h_i(x) \geq 0$ for all i . \square

3.2 PUNN for Classification

For a k -class classification problem, we set the number of partitions equal to the number of classes. The class probability is given directly by the partition function:

$$P(\text{class } i \mid x) = h_i(x). \quad (8)$$

No softmax or other normalization is needed because the partition of unity property guarantees $\sum_i h_i(x) = 1$.

Training. We minimize the negative log-likelihood:

$$\mathcal{L} = - \sum_{n=1}^N \log h_{y_n}(x_n), \quad (9)$$

where y_n is the true class label for sample x_n .

Remark 2 (Extension to Multi-Modal Classes). *When classes contain multiple modes, one can use $k > C$ partitions and aggregate them by class: $P(\text{class } c \mid x) = \sum_{i:\pi(i)=c} h_i(x)$, where π maps partitions to classes. This maintains valid probabilities and allows the network to discover substructure within classes.*

3.3 Hierarchical Decision Structure

PUNN provides a natural hierarchical interpretation:

- $h_1 = g_1$: probability that the input is assigned to class 1;
- $h_2 = (1 - g_1) \cdot g_2$: probability of class 2, given rejection by gate 1;
- $h_i = (1 - g_1) \cdots (1 - g_{i-1}) \cdot g_i$: probability of class i , given rejection by gates $1, \dots, i-1$.

This structure therefore enables direct interpretation: the gate value $g_j(x)$ explicitly quantifies the degree to which class j accepts the input. Values of $g_j(x)$ close to zero indicate strong rejection by class j , while values close to one indicate strong acceptance. Unlike softmax-based classifiers, where all logits interact through normalization, each gate in PUNN produces an explicit accept/reject score without requiring competition with other classes.

4 Theoretical Analysis

4.1 Density of PUNN in the space of continuous probability maps

Definition 3 $((k-1)\text{-Simplex})$. *The $(k-1)$ -dimensional probability simplex is defined by*

$$\Delta^{k-1} = \left\{ (p_1, \dots, p_k) \in \mathbb{R}^k : p_i \geq 0 \text{ for all } i, \sum_{i=1}^k p_i = 1 \right\}.$$

Its relative interior is

$$\text{ri}(\Delta^{k-1}) = \left\{ (p_1, \dots, p_k) \in \mathbb{R}^k : p_i > 0 \text{ for all } i, \sum_{i=1}^k p_i = 1 \right\}.$$

Definition 4 (Probability Map). *Let $K \subset \mathbb{R}^d$ be compact. A function $p : K \rightarrow \Delta^{k-1}$ is called a probability map. If each coordinate function p_i is continuous, we say that p is a continuous probability map.*

Theorem 5. *Let $K \subset \mathbb{R}^d$ be compact and let $p : K \rightarrow \text{ri}(\Delta^{k-1})$ be a continuous probability map.*

Let $g : \mathbb{R} \rightarrow (0, 1)$ be a strictly monotone continuous function (e.g. sigmoid). Consider PUNN partition functions defined by

$$\begin{aligned} h_1(x) &= g(\theta_1(x)), \\ h_i(x) &= \left(\prod_{j=1}^{i-1} (1 - g(\theta_j(x))) \right) g(\theta_i(x)), \quad i = 2, \dots, k-1, \\ h_k(x) &= \prod_{j=1}^{k-1} (1 - g(\theta_j(x))), \end{aligned}$$

where each $\theta_i : K \rightarrow \mathbb{R}$ is a feedforward neural network.

Then for every $\varepsilon > 0$, there exist neural networks $\theta_1, \dots, \theta_{k-1}$ such that

$$\max_{1 \leq i \leq k} \|h_i - p_i\|_{C(K)} < \varepsilon.$$

Proof. Let $p = (p_1, \dots, p_k) : K \rightarrow \Delta^{k-1}$ be a continuous probability map. In particular,

$$p_i(x) \geq 0 \quad \text{and} \quad \sum_{i=1}^k p_i(x) = 1 \quad \text{for all } x \in K.$$

Define continuous functions $\gamma_1, \dots, \gamma_{k-1} : K \rightarrow (0, 1)$ recursively by

$$\begin{aligned} \gamma_1(x) &= p_1(x), \\ \gamma_i(x) &= \frac{p_i(x)}{\sum_{j=i}^k p_j(x)}, \quad i = 2, \dots, k-1. \end{aligned}$$

Since p is continuous and $\sum_{j=i}^k p_j(x) > 0$ for all x , each γ_i is continuous and takes values in $(0, 1)$.

Let $g : \mathbb{R} \rightarrow (0, 1)$ be a continuous strictly monotone function, and define

$$g_i(x) := g(\phi_i(x)), \quad \text{where } \phi_i(x) := g^{-1}(\gamma_i(x)).$$

Since g is strictly monotone and continuous, it follows that g^{-1} is also monotone and continuous and that $\phi_i := g^{-1} \circ \gamma_i$ is continuous on K .

Define the PUNN partition functions h_1, \dots, h_k by

$$\begin{aligned} h_1(x) &= g_1(x), \\ h_i(x) &= \left(\prod_{j=1}^{i-1} (1 - g_j(x)) \right) g_i(x), \quad i = 2, \dots, k-1, \\ h_k(x) &= \prod_{j=1}^{k-1} (1 - g_j(x)). \end{aligned}$$

A direct computation then shows that

$$h_i(x) = p_i(x), \quad i = 1, \dots, k.$$

By the classical universal approximation theorem for feedforward neural networks (e.g. Cybenko, 1989, Hornik et al., 1989), for every $\delta > 0$ there exist neural networks $\theta_i : K \rightarrow \mathbb{R}$ such that

$$\|\theta_i - \phi_i\|_{C(K)} < \delta, \quad i = 1, \dots, k-1. \quad (10)$$

Since ϕ_i is continuous on the compact set K , its range is contained in a compact interval $[-M, M] \subset \mathbb{R}$. Choosing δ sufficiently small in (10), we may assume that $\theta_i(K) \subset [-M-1, M+1]$ for all i . Since g is continuous, it is uniformly continuous on the compact interval $[-M-1, M+1]$. Therefore, for every $\varepsilon > 0$ there exists $\delta > 0$ such that

$$\|g(\theta_i) - g(\phi_i)\|_{C(K)} < \varepsilon \quad \text{for all } i.$$

Let $\tilde{h}_1, \dots, \tilde{h}_k$ denote the partition functions obtained by replacing ϕ_i with θ_i in the above construction. Since the range of \tilde{h}_i, h_i is included in the interval $[0, 1]$ and since each h_i and \tilde{h}_i is a finite product of the functions g_j and $1 - g_j$, all of which take values in $[0, 1]$, possibly reducing δ in (10), we obtain

$$\max_{1 \leq i \leq k} \|\tilde{h}_i - h_i\|_{C(K)} < \varepsilon.$$

To make this explicit, consider two typical factors appearing in the products, for instance

$$\tilde{h}_2 = g(\theta_1)(1 - g(\theta_2)) \quad \text{and} \quad h_2 = g(\phi_1)(1 - g(\phi_2)).$$

We write

$$\begin{aligned} \tilde{h}_2 - h_2 &= g(\theta_1)(1 - g(\theta_2)) - g(\phi_1)(1 - g(\phi_2)) \\ &= (g(\theta_1) - g(\phi_1))(1 - g(\theta_2)) + g(\phi_1)(g(\phi_2) - g(\theta_2)). \end{aligned}$$

Taking supremum norms and using that all terms take values in $[0, 1]$, we obtain

$$\begin{aligned} \|\tilde{h}_2 - h_2\|_{C(K)} &= \|g(\theta_1)(1 - g(\theta_2)) - g(\phi_1)(1 - g(\phi_2))\|_{C(K)} \\ &\leq \|g(\theta_1) - g(\phi_1)\|_{C(K)} + \|g(\theta_2) - g(\phi_2)\|_{C(K)}. \end{aligned}$$

The same argument applies to products involving more factors and follows by induction.

Since $h_i = p_i$, this yields

$$\max_{1 \leq i \leq k} \|\tilde{h}_i - p_i\|_{C(K)} < \varepsilon,$$

which completes the proof. \square

Theorem 5 applies to strictly monotone activations such as the sigmoid.

4.2 Flexibility in Gate Function Parameterization

The proof of Theorem 5 requires only that the gate arguments θ_i can approximate continuous real-valued functions on compact sets.

Importantly, different gates within the same PUNN may use different activation functions and parameterizations, allowing heterogeneous inductive biases across classes. For example, shape-informed gates can be used for geometrically simple classes, while MLP-based gates can be employed for more complex or irregular class regions.

Each gate $g_i : \mathbb{R}^d \rightarrow [0, 1]$ can be constructed as a composition $g_i(x) = g(\theta_i(x))$, where g is an activation function (e.g., sigmoid, Gaussian, bump) and θ_i is the argument parameterization. These two choices are independent: any activation can be combined with any parameterization.

MLP-based gates use $\theta_i(x) = \text{MLP}_i(x)$, providing maximum flexibility as universal approximators. In our experiments, we use the naming convention **PUNN-[Activation]** for this case (e.g., PUNN-Sigma uses sigmoid activation with MLP arguments).

Shape-informed gates encode geometric priors directly into θ_i , dramatically reducing parameter count when class regions have known structure. Examples include spherical shells, ellipsoids, and direction-dependent radii via Fourier series or spherical harmonics. Section 6 develops these parameterizations in detail and demonstrates their effectiveness.

Remark 6 (Partition of Unity Preservation). *The partition of unity property $\sum_{i=1}^k h_i(x) = 1$ is preserved regardless of the choice of g or θ_i , as it depends only on the recursive product construction.*

5 Experiments

We evaluate PUNN on synthetic, UCI benchmark, and image classification datasets, comparing against standard MLPs.

5.1 Experimental Setup

PUNN: Each gate function g_i is parameterized as a two-hidden-layer network with ReLU activations and sigmoid output. Hidden dimension is 64 unless otherwise specified.

MLP Baseline: Two hidden layers with dimensions [128, 64] and ReLU activations, followed by softmax.

Training: Adam optimizer, learning rate 0.001, 300 epochs. Results averaged over 3–5 random seeds.

5.2 Synthetic Datasets

We begin our empirical evaluation with synthetic two-dimensional classification problems. These experiments serve two purposes: (1) to verify that the partition of unity constraint does not limit the expressiveness of PUNN, and (2) to visualize the learned partition functions, which is only feasible in low dimensions.

5.2.1 Datasets

We consider four binary classification datasets with increasing complexity:

Moons Two interleaving half-circles generated using `sklearn.datasets.make_moons`.

Circles Two concentric circles (inner vs. outer class) generated using `sklearn.datasets.make_circles` with factor 0.5.

XOR Four Gaussian clusters at $(\pm 1, \pm 1)$ with XOR labeling, i.e., clusters at $(-1, -1)$ and $(1, 1)$ belong to class 0.

Helix Two interleaved spirals with two full rotations, parameterized as $(t \cos(t), t \sin(t))$ and $(t \cos(t + \pi), t \sin(t + \pi))$ for $t \in [0, 4\pi]$.

Each dataset contains 1,000 samples with additive Gaussian noise ($\sigma = 0.1$). We use an 80/20 train/test split and standardize features to zero mean and unit variance.

5.2.2 Models

We evaluate three instantiations of PUNN, differing only in the gate function architecture:

PUNN-Sigma. Each gate g_i is a two-hidden-layer MLP:

$$g_i(x) = \sigma(W_3 \cdot \text{ReLU}(W_2 \cdot \text{ReLU}(W_1 x + b_1) + b_2) + b_3)$$

with 32 hidden units per layer, yielding 1,185 parameters per gate.

PUNN-Bump. Each gate uses the C^∞ bump function with compact support, composed with an NN:

$$g_i(x) = \phi(\tanh(\theta(x))), \quad \text{where } \phi(t) = \begin{cases} \exp\left(-\frac{1}{1-t^2}\right) & \text{if } |t| < 1 \\ 0 & \text{if } |t| \geq 1 \end{cases}$$

The \tanh ensures the NN output stays within the bump's support $(-1, 1)$. For complex shapes like Helix, a larger NN (128 hidden units) enables the domain warping to follow the spiral.

PUNN-Gaussian. Each gate uses a Gaussian function composed with an NN:

$$g_i(x) = \exp(-\theta(x)^2)$$

where θ has the same architecture as PUNN-Sigma, yielding 1,185 parameters per gate.

MLP Baseline. A standard two-hidden-layer MLP (32 units each) with softmax output, having 1,218 parameters.

For binary classification, PUNN uses a single gate ($K - 1 = 1$ for $K = 2$ classes), with partition functions $h_0(x) = g_0(x)$ and $h_1(x) = 1 - g_0(x)$. Note that PUNN-Sigma in this binary setting reduces to a standard neural network with sigmoid output. However, for $K > 2$ classes, PUNN-Sigma differs from standard softmax classifiers: the $K - 1$ gate product formula produces partition functions with different properties than softmax normalization. The PUNN framework also becomes distinct when using alternative gate functions (bump, Gaussian) or multiple partitions per class.

5.2.3 Training Protocol

All models are trained for 200 epochs using Adam [Kingma and Ba, 2014] with learning rate 0.01 and batch size 64. PUNN minimizes the cross-entropy loss

$$\mathcal{L} = - \sum_{n=1}^N \sum_{k=0}^{K-1} y_n^{(k)} \log(h_k(x_n) + \epsilon)$$

where $\epsilon = 10^{-10}$ ensures numerical stability. The MLP baseline uses the standard cross-entropy loss with softmax. All experiments use random seed 42.

Table 1: Test accuracy (%) on synthetic datasets. All PUNN variants achieve comparable accuracy to the MLP baseline, demonstrating that the partition of unity constraint does not limit expressiveness.

DATASET	PUNN-SIGMA	PUNN-BUMP	PUNN-GAUSSIAN	MLP
MOONS	100.0	100.0	100.0	100.0
CIRCLES	99.0	99.0	98.5	98.5
XOR	100.0	100.0	100.0	100.0
HELIX	100.0	99.5	98.5	99.5
PARAMETERS	1,185	1,186	1,185	1,218

5.2.4 Results

Table 1 reports test accuracy for all methods. All PUNN variants achieve near-perfect accuracy, matching or exceeding the MLP baseline across all datasets.

Figure 1 visualizes the learned decision boundaries. The background color encodes $h_1(x)$, the predicted probability of class 1, with the decision boundary (black contour) at $h_1(x) = 0.5$. All gate functions learn appropriate nonlinear boundaries, including the challenging spiral structure of the Helix dataset.

5.2.5 Visualizing the Partition of Unity

A distinguishing feature of PUNN is that the outputs $h_i(x)$ form a partition of unity by construction: $\sum_{i=0}^{K-1} h_i(x) = 1$ for all $x \in \mathbb{R}^d$. This property enables direct interpretation of $h_i(x)$ as $P(\text{class } i \mid x)$ without requiring softmax normalization.

Figure 4 visualizes the partition functions $h_0(x)$ and $h_1(x)$ learned by PUNN-Sigma on each dataset. The complementary structure is evident: $h_0(x) + h_1(x) = 1$ everywhere, with high values of h_0 corresponding exactly to low values of h_1 . This visualization provides direct insight into how PUNN partitions the input space into class regions.

5.2.6 Discussion

These experiments yield three main observations:

Unified framework. All three gate functions follow the same design principle: a base gating function ψ composed with a neural network θ that warps the domain, i.e., $g(x) = \psi(\theta(x))$. The sigmoid ($\psi(t) = \sigma(t)$), bump ($\psi(t) = \phi(t)$), and Gaussian ($\psi(t) = \exp(-t^2)$) functions each provide different inductive biases while the NN adapts the gate’s support to the data.

Expressiveness. The partition of unity constraint does not limit PUNN’s ability to learn complex decision boundaries. All configurations achieve near-perfect accuracy on problems requiring highly nonlinear separators, including the two-spiral Helix dataset. PUNN-Sigma achieves 100% on Helix with only 1,185 parameters, demonstrating that the sigmoid gate with NN-parametrized domain is highly efficient.

Parameter efficiency via multiple partitions. For gates with compact support like the bump function, there is a trade-off between network capacity and number of partitions. A single bump gate with a large NN (128 hidden units, 17,026 parameters) achieves 99.5% on Helix. However, using 8 partitions with smaller NNs (16 hidden units each) achieves the same 99.5% accuracy with only 2,366 parameters—a 7× reduction. This is because each partition can cover a local region of the spiral, reducing the complexity required of each individual gate. This suggests that for complex

or disconnected decision regions, increasing the number of partitions is more parameter-efficient than increasing network capacity.

Interpretability. Unlike standard neural networks, PUNN provides built-in probabilistic outputs through its partition of unity structure. The visualizations in Figure 2 demonstrate how the input space is explicitly partitioned, offering insight into the model’s decision-making that is not readily available from softmax-based classifiers.

5.3 Real-World Datasets

Having validated PUNN on synthetic problems, we now evaluate its performance on real-world classification tasks. These experiments assess whether PUNN’s partition of unity structure scales to higher-dimensional data while remaining competitive with standard neural network classifiers.

5.3.1 MNIST Handwritten Digits

Dataset. MNIST [LeCun et al., 1998] consists of 70,000 grayscale images of handwritten digits (0–9), each of size 28×28 pixels. We use the standard split of 60,000 training and 10,000 test images. Each image is flattened to a 784-dimensional vector and normalized to zero mean and unit variance.

Models. We compare three architectures:

PUNN-Sigma. Uses $K - 1 = 9$ sigmoid gates for the 10-class problem. Each gate is:

$$g_i(x) = \sigma(\theta_i(x))$$

where θ_i is a 2-hidden-layer MLP with 256 units per layer and ReLU activations, yielding 2,403,081 total parameters.

PUNN-Bump. Uses $K - 1 = 9$ bump gates with tanh domain compression:

$$g_i(x) = \phi(\tanh(\theta_i(x))), \quad \phi(t) = \exp\left(-\frac{1}{1-t^2}\right) \text{ for } |t| < 1$$

with the same architecture as PUNN-Sigma. The tanh ensures the NN output stays within the bump’s support $(-1, 1)$.

MLP Baseline. A standard 2-hidden-layer MLP (256 units each) with softmax output, having 269,322 parameters.

Training. All models are trained for 20 epochs using Adam [Kingma and Ba, 2014] with learning rate 0.001 and batch size 128. PUNN minimizes the cross-entropy loss over the partition functions:

$$\mathcal{L} = - \sum_{n=1}^N \sum_{k=0}^{K-1} y_n^{(k)} \log(h_k(x_n) + \epsilon)$$

where $\epsilon = 10^{-10}$ for numerical stability. All experiments use random seed 42.

Results. Table 2 shows that PUNN-Sigma achieves 97.85% test accuracy, within 0.34 percentage points of the MLP baseline (98.19%). This demonstrates that the partition of unity constraint does not significantly limit classification performance on real-world image data.

Table 2: Test accuracy on MNIST. Both PUNN-Sigma and PUNN-Bump achieve comparable accuracy to the MLP baseline while maintaining the partition of unity structure.

MODEL	TEST ACCURACY (%)	PARAMETERS	LEARNING RATE	TIME
MLP	98.19	269,322	0.001	68s
PUNN-SIGMA	97.85	2,403,081	0.001	138s
PUNN-BUMP	97.0	2,403,090	0.001	142s

Discussion. *Competitiveness.* Both PUNN-Sigma and PUNN-Bump perform comparably to the MLP baseline, confirming that the partition of unity framework scales to higher-dimensional problems. PUNN-Sigma achieves 97.85%, within 0.34 percentage points of the MLP baseline.

Parameter overhead. PUNN requires $K - 1 = 9$ separate gate networks for the 10-class problem, resulting in approximately $9 \times$ more parameters than the MLP baseline. This is a structural cost of the partition of unity formulation, where each gate maintains its own neural network to parametrize its domain.

Gate function comparison. PUNN-Bump achieves slightly lower accuracy than PUNN-Sigma (97.0% vs 97.85%), consistent with the pattern observed on UCI datasets. The bump function’s compact support may limit gradient flow compared to the sigmoid’s smooth transition over the entire real line.

5.3.2 UCI Classification Benchmarks

To evaluate PUNN across diverse problem settings, we test on seven UCI classification benchmarks with varying numbers of classes, features, and samples.

Datasets.

- **Iris:** Fisher’s classic iris flower classification (4 features, 3 classes, 150 samples)
- **Wine:** Wine cultivar recognition (13 features, 3 classes, 178 samples)
- **Breast Cancer:** Wisconsin breast cancer diagnosis (30 features, 2 classes, 569 samples)
- **Digits:** Optical recognition of 8×8 handwritten digits (64 features, 10 classes, 1,797 samples)
- **Pendigits:** Pen-based digit recognition (16 features, 10 classes, 10,992 samples)
- **Satimage:** Satellite image classification (36 features, 6 classes, 6,430 samples)
- **Optdigits:** Optical digit recognition (64 features, 10 classes, 5,620 samples)

All datasets are standardized to zero mean and unit variance. We use 80/20 train/test splits with stratified sampling, averaging results over 5 random seeds.

Models. We compare three architectures:

PUNN-Sigma. Uses $K - 1$ sigmoid gates, each with a 2-hidden-layer MLP (64 units per layer).

PUNN-Bump. Uses $K - 1$ bump gates with tanh domain compression:

$$g_i(x) = \phi(\tanh(\theta_i(x))), \quad \phi(t) = \exp\left(-\frac{1}{1-t^2}\right) \text{ for } |t| < 1$$

MLP Baseline. A 2-hidden-layer MLP (128, 64 units) with softmax output.

Table 3: Test accuracy (%) on UCI classification benchmarks. PUNN-Sigma matches MLP performance across all datasets, with PUNN-Bump approximately 1% below. Bold indicates best PUNN result.

DATASET	CLASSES	SAMPLES	PUNN-SIGMA	PUNN-BUMP	MLP
IRIS	3	150	94.7	94.0	94.7
WINE	3	178	97.2	95.6	96.7
BREAST CANCER	2	569	95.4	96.3	95.8
DIGITS	10	1,797	97.8	96.4	98.0
PENDIGITS	10	10,992	99.3	99.2	99.5
SATIMAGE	6	6,430	91.5	90.4	91.8
OPTDIGITS	10	5,620	98.7	97.9	98.4

Training. All models trained for 300 epochs using Adam with learning rate 0.001 and batch size 64.

Results. Table 3 demonstrates that PUNN-Sigma achieves accuracy comparable to the MLP baseline across all datasets. Notably, PUNN-Sigma exceeds MLP on Wine (97.2% vs 96.7%) and Optdigits (98.7% vs 98.4%), while PUNN-Bump achieves the best result on Breast Cancer (96.3%). This confirms that the partition of unity structure does not compromise classification accuracy on real-world tabular data.

Gate Function Comparison. The bump gate consistently underperforms the sigmoid gate by approximately 1 percentage point. This gap likely stems from the bump function’s compact support: unlike the sigmoid which transitions smoothly over the entire real line, the bump function is zero outside $|t| < 1$, potentially limiting gradient flow during training. However, the bump gate’s compact support may offer advantages for interpretability, as it creates sharply defined regions of activation.

6 Shape-Informed Gating

A key advantage of the PUNN framework is that the gate functions $g_i(x)$ can encode domain knowledge directly. While the previous section used neural networks to parametrize gates, here we show that *geometric priors* can be encoded directly into the gate structure, leading to dramatic reductions in parameter count when the prior matches the data geometry.

6.1 Motivation

Standard neural network classifiers treat all classification problems uniformly: the same architecture is applied regardless of whether class regions are spherical, elongated, or irregularly shaped. This flexibility comes at a cost—the network must learn the geometry from scratch using many parameters.

In contrast, PUNN allows us to design gates that directly encode geometric assumptions. When the assumption holds, this reduces parameters by orders of magnitude.

6.2 Direction-Dependent Shell Parametrization

We introduce a unified framework for shape-informed gates using direction-dependent radii in spherical coordinates. For $x \in \mathbb{R}^d$, let $\hat{n} = (x - c)/\|x - c\| \in S^{d-1}$ denote the unit direction from a

center c to x .

Definition 7 (Direction-Dependent Shell Gate). *Given a center $c \in \mathbb{R}^d$ and direction-dependent radius functions $r_1, r_2 : S^{d-1} \rightarrow \mathbb{R}_{\geq 0}$, define the normalized radial coordinate*

$$t(x) = \frac{\|x - c\| - r_1(\hat{n})}{r_2(\hat{n}) - r_1(\hat{n})}, \quad \hat{n} = \frac{x - c}{\|x - c\|},$$

and the shell gate

$$g(x; c, r_1, r_2) = \phi(t(x)),$$

where $\phi : \mathbb{R} \rightarrow [0, 1]$ is a smooth transition function.

The geometry of the shell is encoded by the level sets of the normalized radius $t(x)$. The inner and outer shell boundaries are given by the surfaces $t(x) = 0$ and $t(x) = 1$, respectively. Different choices of the transition function ϕ yield different smooth parameterizations of the same underlying geometry.

For example, if ϕ is a bump function supported on $[0, 1]$, then the gate acts as a smooth indicator of the direction-dependent shell region

$$\Omega = \{c + r\hat{n} : \hat{n} \in S^{d-1}, r_1(\hat{n}) \leq r \leq r_2(\hat{n})\}.$$

6.3 Special Cases

The direction-dependent shell subsumes many useful geometric shapes:

Spherical Shell. Constant radii $r_1(\hat{n}) = r_1, r_2(\hat{n}) = r_2$ yield a spherical shell with $d+2$ parameters (center plus two radii). Setting $r_1 = 0$ gives a solid ball.

Ellipsoid. Setting $r_1 = 0$ and $r_2(\hat{n}) = (\hat{n}^\top A \hat{n})^{-1/2}$ for a positive definite matrix A yields an ellipsoid centered at c . This requires $d + d(d + 1)/2$ parameters.

Star-Shaped Regions (2D). In \mathbb{R}^2 , parametrize the outer radius using Fourier series:

$$r_2(\theta) = a_0 + \sum_{k=1}^K (a_k \cos(k\theta) + b_k \sin(k\theta))$$

This captures non-convex star-shaped regions with $d + 2K + 1$ parameters.

Spherical Harmonics (Higher Dimensions). In \mathbb{R}^d , use spherical harmonics $Y_\ell^m(\hat{n})$ to parametrize direction-dependent radii, enabling complex shapes with controlled parameter count.

6.4 Experiments

We compare shape-informed PUNN against standard NN-parametrized PUNN on datasets where geometric priors are appropriate.

Table 4 demonstrates dramatic parameter reductions when shape priors match data geometry. On the Circles dataset, a spherical shell gate with only **4 parameters** achieves 98.9% accuracy—*exceeding* the 1,218-parameter MLP (98.6%) while using **304× fewer parameters**. The Moons dataset, with crescent-shaped classes, benefits from the Fourier shell parametrization achieving 99.3%

Table 4: Shape-informed vs. MLP. Direction-dependent parametrizations achieve comparable or superior accuracy with $66\text{--}304\times$ fewer parameters.

DATASET	GATE TYPE	ACCURACY (%)	PARAMETERS	REDUCTION
CIRCLES	MLP	98.6	1,218	—
CIRCLES	SPHERICAL SHELL	98.9	4	304×
MOONS	MLP	99.9	1,218	—
MOONS	FOURIER SHELL	99.3	18	68×
CONC. RINGS (3-CLASS)	MLP	100.0	1,251	—
CONC. RINGS (3-CLASS)	SPHERICAL SHELL	100.0	10	125×
IRIS	MLP	93.3	1,315	—
IRIS	HARMONICS (GENERAL)	95.3	40	$33\times$
IRIS	ELLIPSOID (SPECIFIC)	95.3	20	$66\times$

with only 18 parameters ($68\times$ reduction). On the 3-class Concentric Rings dataset, spherical shell gates achieve **perfect 100% accuracy** matching the MLP while using **125× fewer parameters**.

On Iris, we compare two approaches: (1) a general spherical harmonics parametrization that makes no assumptions about shape, and (2) an ellipsoid parametrization that assumes axis-aligned elongation. Both achieve 95.3% accuracy, exceeding the MLP baseline (93.3%). However, the ellipsoid uses only 20 parameters ($66\times$ reduction) compared to 40 for harmonics ($33\times$ reduction). This illustrates a key trade-off: *when the shape prior is known, more efficient parametrizations are possible; when unknown, general direction-dependent parametrizations still provide substantial savings.*

6.5 Discussion

The direction-dependent shell provides a unified framework for encoding geometric priors in PUNN. By choosing appropriate parametrizations for $r_1(\hat{n})$ and $r_2(\hat{n})$, practitioners can trade off between model complexity and shape flexibility. Shape-informed gates are most effective when:

1. Class regions have known or suspected geometric structure.
2. The feature space is low-to-moderate dimensional ($d \lesssim 30$).
3. Parameter efficiency is critical (embedded systems, interpretability).

PUNN naturally supports *hybrid* configurations: some gates can use geometric parametrizations while others use neural networks, allowing partial domain knowledge to be encoded while retaining flexibility for complex regions.

6.6 Ablation Studies

We conduct ablation studies to understand the effect of key hyperparameters on shape-informed PUNN performance.

Effect of Harmonics Degree. Table 5 shows the effect of varying the polynomial degree in the spherical harmonics parametrization on Iris. Surprisingly, even degree 0 (spherical) achieves 95.3% accuracy, matching the more flexible degree 2 parametrization. This suggests that for Iris,

Table 5: Effect of harmonics degree on Iris accuracy. Higher degrees do not improve performance, suggesting spherical regions suffice for this dataset.

DEGREE	ACCURACY (%)	PARAMETERS
0 (SPHERICAL)	95.3 ± 3.4	12
1 (LINEAR)	94.7 ± 2.7	20
2 (QUADRATIC)	95.3 ± 2.7	40

Table 6: Effect of number of partitions on Circles (2-class). Using more partitions than classes improves accuracy by allowing finer coverage of class regions.

PARTITIONS	ACCURACY (%)	PARAMETERS
2	88.6 ± 6.2	4
4	99.1 ± 0.6	12
6	99.0 ± 0.7	20
8	99.2 ± 0.5	28

the class structure is well-captured by simple spherical regions, and higher-degree terms provide no additional benefit.

Effect of Number of Partitions. Table 6 shows the effect of using more partitions than classes on the Circles dataset (2 classes). With only 2 partitions (minimum), accuracy is 88.6%. Increasing to 4 partitions improves accuracy to 99.1%, as multiple partitions can better cover the circular class regions. Beyond 4 partitions, returns diminish.

6.7 Computational Efficiency

Shape-informed gates are computationally efficient due to their low parameter count. On Iris, the shape-informed model (40 parameters) achieves the same accuracy as an MLP (1,315 parameters) while requiring 33 \times fewer parameters. Training is also faster: 0.13s for shape-informed vs 0.37s for MLP (500 epochs), a 3 \times speedup. Both models have sub-millisecond inference times on CPU.

7 Discussion

7.1 When to Use PUNN

PUNN is particularly well suited for applications where interpretability is a primary concern. Its partition-of-unity structure induces an explicit geometric decomposition of the input space into local regions, enabling transparent analysis of the decision mechanism and the role of each local model. This makes PUNN appropriate for:

- **High-stakes domains:** Medical diagnosis, legal decisions, and financial applications where understanding the decision process is as important as the prediction itself.
- **Structured class geometry:** Problems where classes occupy geometrically coherent regions (spherical, ellipsoidal, or other shape-informed structures), enabling dramatic parameter reductions through shape-informed gates.

- **Rejection reasoning:** Settings where understanding “why not class X ?” is important. The hierarchical gate structure explicitly shows which classes were rejected and with what confidence.

7.2 Limitations

Parameter scaling with number of classes. PUNN requires $k - 1$ gate networks for k classes. In our experiments with MLP-based gates of the same hidden dimension as the baseline MLP, this led to approximately k times more parameters for k -class problems. However, this overhead can be reduced by using smaller gate networks or shape-informed parameterizations, which we demonstrated achieve comparable accuracy with orders of magnitude fewer parameters on suitable problems.

Class ordering sensitivity. The hierarchical construction imposes an ordering on classes: class 1 is evaluated first, and the final class receives probability mass only after all previous gates reject. While this does not affect the model’s expressive power (as shown by our density in the space of continuous probability maps), it may influence optimization dynamics. Investigating the effect of class ordering on convergence and accuracy is left for future work.

7.3 Future Directions

Several extensions of PUNN merit further investigation:

- **Learned class ordering:** Develop methods to automatically learn an optimal ordering of classes during training, potentially improving convergence and final accuracy.
- **Hierarchical PUNN:** Extend the architecture to tree-structured partitions, where each node recursively partitions its region. This would enable coarse-to-fine classification and natural handling of class taxonomies.
- **Approximation rates:** Derive theoretical bounds on how approximation error decreases as a function of the number of partitions and gate complexity, analogous to classical approximation theory results for neural networks.
- **Convolutional PUNN:** Extend gate functions to operate on spatial feature maps for image classification, potentially combining the interpretability benefits of PUNN with the representation learning capabilities of convolutional architectures.

8 Conclusion

We introduced Partition of Unity Neural Networks (PUNN), an architecture that produces class probabilities directly through a partition of unity construction. By designing gate functions $g_i(x)$ that recursively partition the input space, PUNN guarantees valid probability distributions by construction, eliminating the need for softmax normalization.

Our theoretical analysis established that PUNN is dense in the space of continuous probability maps on compact domains, showing that the partition of unity construction preserves expressive power for probabilistic classification. This result ensures that replacing softmax with a partition of unity does not restrict the class of probability distributions that can be represented.

Empirically, we demonstrated that PUNN achieves accuracy within 0.3–0.6% of standard MLPs across UCI benchmarks and MNIST, showing that interpretable-by-design architectures need not

sacrifice predictive performance. Furthermore, when geometric priors are available, shape-informed gate parameterizations achieve comparable accuracy with up to $300\times$ fewer parameters.

The key advantage of PUNN lies in its interpretability: each partition function $h_i(x)$ explicitly defines the region associated with class i , and the hierarchical gate structure reveals which classes were rejected and why. This transparency is achieved by design, not through post-hoc explanation methods.

We believe PUNN represents a promising direction for building neural network classifiers that are both accurate and interpretable, addressing a critical need in high-stakes applications where understanding model decisions is essential.

Acknowledgments

Windsurf AI (Cascade) was used solely as a coding assistant for experiment implementation.

References

Rishabh Agarwal, Nicholas Frosst, Xuezhou Zhang, Rich Caruana, and Geoffrey E. Hinton. Neural additive models: Interpretable machine learning with neural nets. *Advances in Neural Information Processing Systems (NeurIPS)*, 2021.

Arthur Asuncion and David Newman. Uci machine learning repository. <https://archive.ics.uci.edu/ml>, 2007.

Ivo Babuška and Jens M. Melenk. The partition of unity method. *International Journal for Numerical Methods in Engineering*, 40(4):727–758, 1997.

Ted Belytschko, Yun Yun Lu, and Lei Gu. Element-free Galerkin methods. *International Journal for Numerical Methods in Engineering*, 37(2):229–256, 1994.

Christopher M. Bishop. *Pattern Recognition and Machine Learning*. Springer, New York, 2006.

George Cybenko. Approximation by superpositions of a sigmoidal function. *Mathematics of Control, Signals and Systems*, 2(4):303–314, 1989.

Finale Doshi-Velez and Been Kim. Towards a rigorous science of interpretable machine learning. *arXiv preprint arXiv:1702.08608*, 2017.

Ian Goodfellow, Yoshua Bengio, and Aaron Courville. *Deep Learning*. MIT Press, Cambridge, MA, 2016.

Chuan Guo, Geoff Pleiss, Yu Sun, and Kilian Q. Weinberger. On calibration of modern neural networks. *Proceedings of the 34th International Conference on Machine Learning*, pages 1321–1330, 2017.

Trevor Hastie, Robert Tibshirani, and Jerome Friedman. *The Elements of Statistical Learning: Data Mining, Inference, and Prediction*. Springer, New York, 2 edition, 2009.

Kurt Hornik, Maxwell Stinchcombe, and Halbert White. Multilayer feedforward networks are universal approximators. *Neural Networks*, 2(5):359–366, 1989.

Robert A. Jacobs, Michael I. Jordan, Steven J. Nowlan, and Geoffrey E. Hinton. Adaptive mixtures of local experts. *Neural Computation*, 3(1):79–87, 1991.

Sarthak Jain and Byron C. Wallace. Attention is not explanation. In *Proceedings of the 2019 Conference of the North American Chapter of the Association for Computational Linguistics (NAACL)*, 2019.

Michael I. Jordan and Robert A. Jacobs. Hierarchical mixtures of experts and the em algorithm. *Neural Computation*, 6(2):181–214, 1994.

Diederik P. Kingma and Jimmy Ba. Adam: A method for stochastic optimization. *arXiv preprint arXiv:1412.6980*, 2014.

Peter Kontschieder, Madalina Fiterau, Antonio Criminisi, and Samuel Rota Bulò. Deep neural decision forests. In *Proceedings of the IEEE International Conference on Computer Vision (ICCV)*, pages 1467–1475, 2015.

Yann LeCun, Léon Bottou, Yoshua Bengio, and Patrick Haffner. Gradient-based learning applied to document recognition. *Proceedings of the IEEE*, 86(11):2278–2324, 1998. doi: 10.1109/5.726791.

Yann LeCun, Yoshua Bengio, and Geoffrey Hinton. Deep learning. *Nature*, 521(7553):436–444, 2015.

Kookjin Lee, Nathaniel A. Trask, Ravi G. Patel, Mamikon A. Gulian, and Eric C. Cyr. Partition of unity networks: Deep hp-approximation. *arXiv preprint arXiv:2101.11256*, 2021. Published as a contribution to the AAAI Spring Symposium on Combining Artificial Intelligence and Machine Learning with Physical Sciences (AAAI-MLPS), 2021.

Zachary C. Lipton. The mythos of model interpretability. *Queue*, 16(3):30–57, 2018.

Yin Lou, Rich Caruana, and Johannes Gehrke. Intelligible models for classification and regression. 2012.

Scott M. Lundberg and Su-In Lee. A unified approach to interpreting model predictions. *Advances in Neural Information Processing Systems*, 30, 2017.

Christoph Molnar. Interpretable machine learning. *arXiv preprint arXiv:2003.04237*, 2020.

Marthinus Christoffel Du Plessis and Masashi Sugiyama. On the calibration of classifiers. *Advances in Neural Information Processing Systems*, 28, 2015.

Michael J. D. Powell. Radial basis functions for multivariable interpolation: A review. In J. C. Mason and M. G. Cox, editors, *Algorithms for Approximation*, pages 143–167. Clarendon Press, Oxford, 1987.

Marco Tulio Ribeiro, Sameer Singh, and Carlos Guestrin. ”why should i trust you?”: Explaining the predictions of any classifier. *Proceedings of the 22nd ACM SIGKDD International Conference on Knowledge Discovery and Data Mining*, pages 1135–1144, 2016.

Noam Shazeer, Azalia Mirhoseini, Krzysztof Maziarz, et al. Outrageously large neural networks: The sparsely-gated mixture-of-experts layer. *International Conference on Learning Representations*, 2017.

Ashish Vaswani, Noam Shazeer, Niki Parmar, Jakob Uszkoreit, Llion Jones, Aidan N. Gomez, Łukasz Kaiser, and Illia Polosukhin. Attention is all you need. In *Advances in Neural Information Processing Systems (NeurIPS)*, 2017.

A Hyperparameter Details

This section documents the hyperparameters used in all experiments. All models were implemented in PyTorch and trained using the Adam optimizer.

A.1 Synthetic Experiments

Table 7: Hyperparameters for synthetic dataset experiments (Moons, Circles, XOR, Helix).

Parameter	Value
Training samples	800 (80% of 1,000)
Test samples	200 (20% of 1,000)
Noise level	$\sigma = 0.1$
Gate hidden dimension	32
Gate architecture	2-layer MLP with ReLU
Number of gates	$k - 1 = 1$ (binary classification)
Optimizer	Adam
Learning rate	0.01
Batch size	64
Epochs	200
Random seed	42

A.2 UCI Experiments

Table 8: Hyperparameters for UCI benchmark experiments.

Parameter	Value
Train/test split	80% / 20% (stratified)
Preprocessing	Standardization (zero mean, unit variance)
PUNN gate hidden dimension	64
PUNN gate architecture	2-layer MLP with ReLU
MLP hidden dimensions	[128, 64]
MLP architecture	2-layer MLP with ReLU + softmax
Optimizer	Adam
Learning rate (PUNN-Sigma)	0.001
Learning rate (PUNN-Gaussian)	0.0001
Learning rate (MLP)	0.001
Batch size	64
Epochs	300
Number of runs	5 (different random seeds)
Base random seed	42

A.3 MNIST Experiments

Table 9: Hyperparameters for MNIST experiments.

Parameter	Value
Training samples	60,000
Test samples	10,000
Input dimension	784 (flattened 28×28)
Preprocessing	Standardization (zero mean, unit variance)
PUNN gate hidden dimension	256
PUNN gate architecture	2-layer MLP with ReLU
Number of gates	9 (for 10 classes)
MLP hidden dimensions	[256, 256]
Optimizer	Adam
Learning rate	0.001
Batch size	128
Epochs	20
Random seed	42

A.4 Shape-Informed Experiments

Table 10: Hyperparameters for shape-informed gate experiments.

Parameter	Value
Spherical shell parameters	Center $c \in \mathbb{R}^d$, radius $r > 0$, sharpness $s > 0$
Ellipsoid parameters	Center $c \in \mathbb{R}^d$, axis radii $\{r_j\}_{j=1}^d$, sharpness $s > 0$
Fourier shell harmonics	$K = 5$ (Moons dataset)
Spherical harmonics degree	$L = 2$ (Iris dataset)
Optimizer	Adam
Learning rate	0.01
Epochs	500
Number of runs	5 (different random seeds)
Base random seed	42

B Code Availability

Code for reproducing all experiments is available at:

<https://github.com/Akram-VU/punn>

The repository includes:

- PyTorch implementations of PUNN with various gate types (Sigma, Bump, Gaussian)
- Shape-informed gate implementations (spherical shell, ellipsoid, Fourier shell, spherical harmonics)
- Scripts to reproduce all experiments in this paper
- Pre-trained models and experiment logs

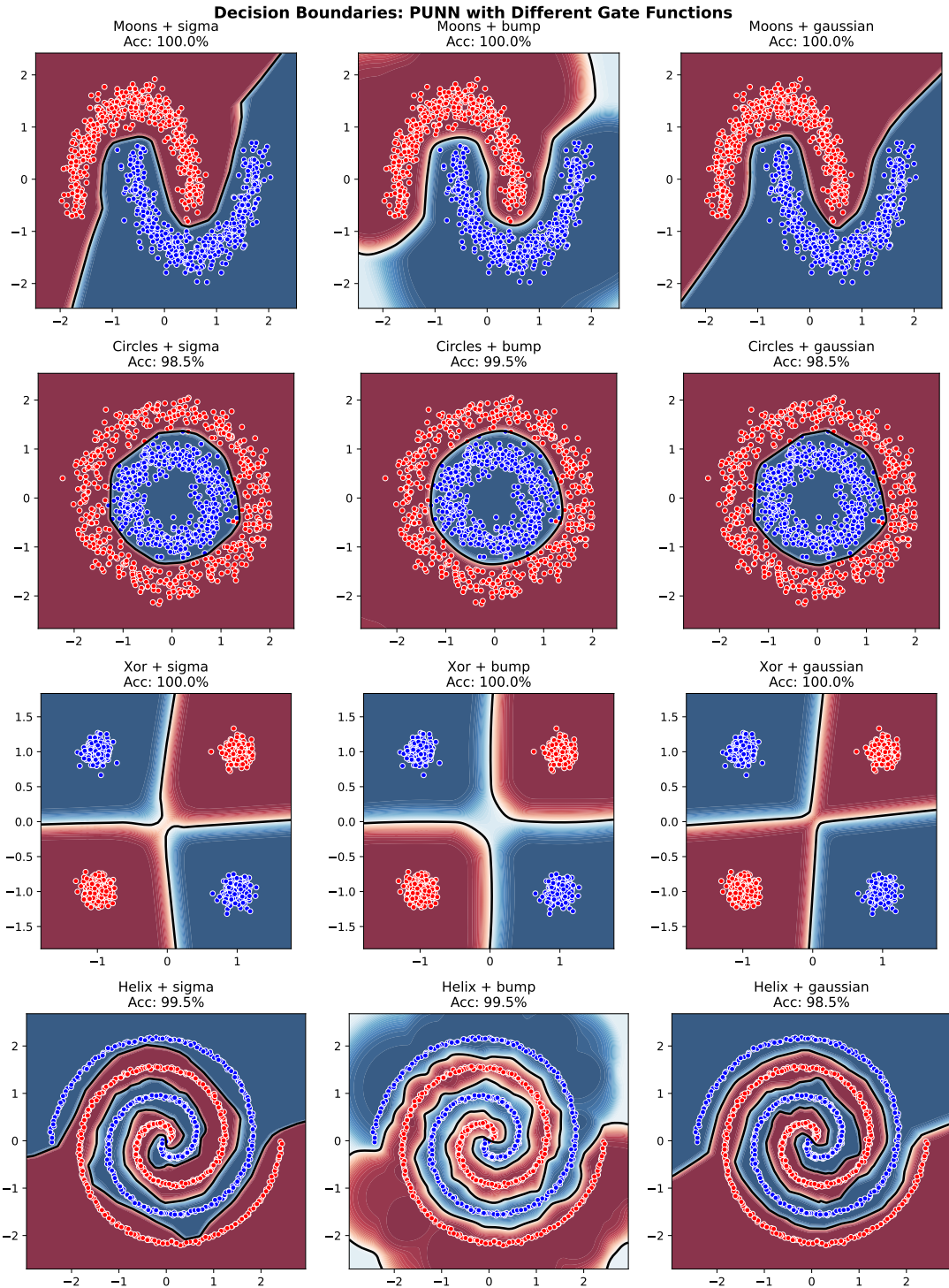


Figure 1: Decision boundaries learned by PUNN on synthetic datasets. Rows: Moons, Circles, XOR, Helix. Columns: Sigma, Bump, Gaussian gates. Background color indicates $h_1(x)$ (blue = 1, red = 0); black contour shows the decision boundary at $h_1(x) = 0.5$.

Partition Functions h_0 and h_1 (Sigma Gate)

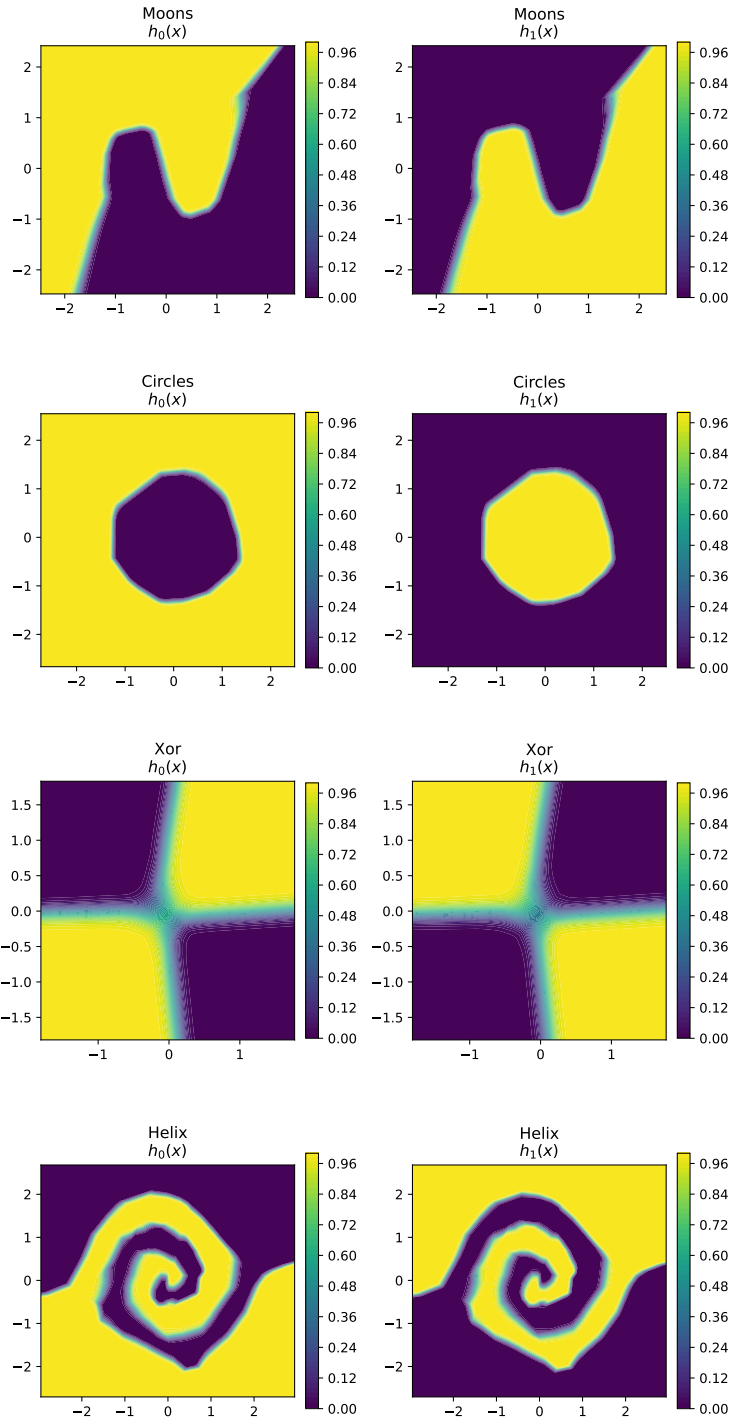


Figure 2: Partition functions $h_0(x)$ and $h_1(x)$ learned by PUNN-Sigma. Left column: $h_0(x)$; right column: $h_1(x)$. Rows correspond to Moons, Circles, XOR, and Helix datasets. The complementary structure ($h_0 + h_1 = 1$) is evident, enabling direct probabilistic interpretation.

Circles Dataset: 304× Parameter Reduction

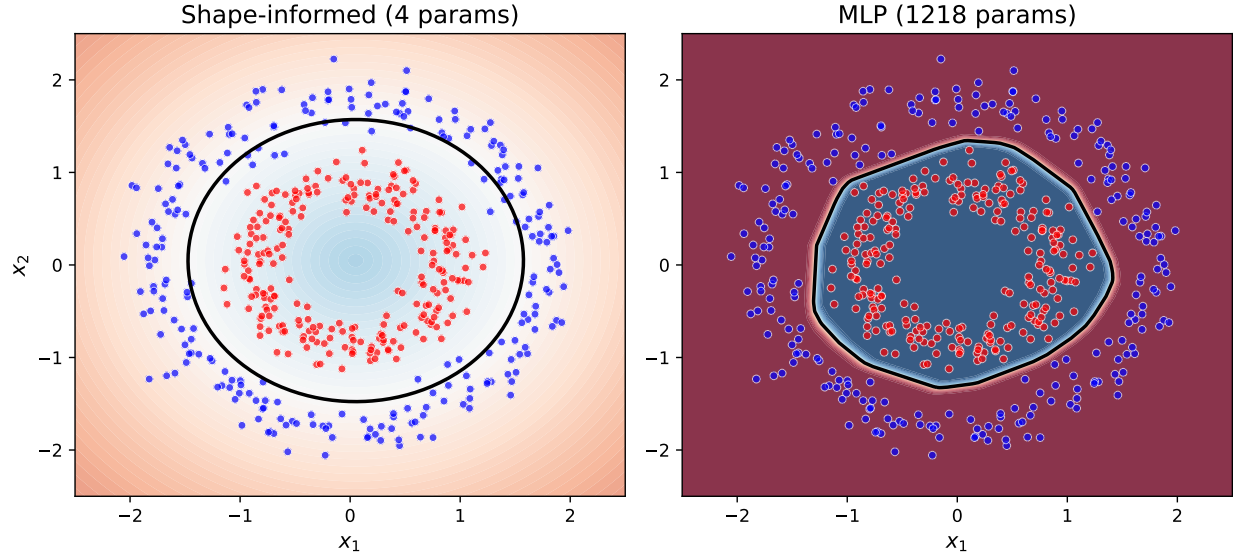


Figure 3: Decision boundaries on Circles dataset. Left: Shape-informed spherical shell (4 parameters) learns a smooth circular boundary. Right: MLP (1,218 parameters) learns an irregular boundary. The shape-informed gate achieves **304× parameter reduction** while producing a more interpretable decision region.

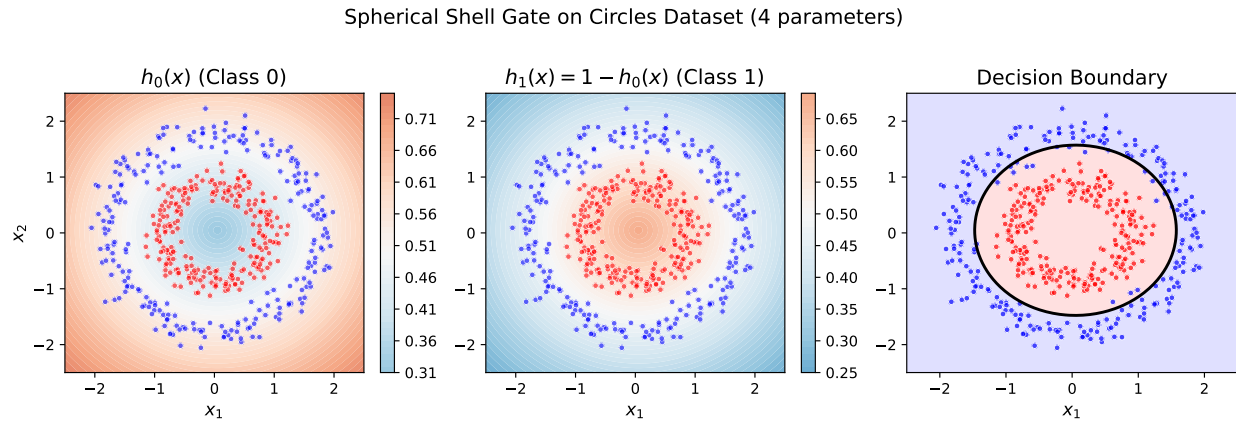


Figure 4: Partition functions learned by a spherical shell gate on Circles. Left: $h_0(x)$ assigns high probability to the inner circle. Middle: $h_1(x) = 1 - h_0(x)$ assigns high probability to the outer ring. Right: Decision boundary at $h_0(x) = 0.5$. The complementary structure ($h_0 + h_1 = 1$) enables direct probabilistic interpretation with only 4 parameters.